MODELING AND OPTIMIZATION OF FLEXIBLE LIGHT-EMITTING DIODE ARRAY FOR UNIFORM LIGHT DISTRIBUTION IN PHOTOTHERAPEUTIC APPLICATIONS

A Thesis

by

BLANCHE TER HOFSTEDE

Submitted to the Graduate and Professional School of
Texas A&M University
in partial fulfillment of the requirements for the degree of

MASTER OF SCIENCE

Chair of Committee,	Kristen C. Maitland
Committee Members,	Limei Tian
	Christi K. Madsen
Head of Department,	Michael J. McShane

August 2021

Major Subject: Biomedical Engineering

ABSTRACT

Phototherapy is the use of light ranging from ultraviolet to near-infrared wavelengths for clinical applications such as treatment of acne, wound healing, and inactivation of bacteria and fungi. The application is dependent on the wavelengths used and required penetration depth due to the nature of light-tissue interactions. Light emitting diodes (LEDs) assembled into arrays have become a popular light source in phototherapy because of their high efficiency and lower costs replacing expensive lasers and bulky, inefficient filtered lamps. However, when illuminating close to the skin for therapeutic applications, LEDs form concentrated areas of light causing uneven illumination on the treatment area that has been shown to reduce the efficacy of phototherapy.

In this work, an optical model of a previously fabricated flexible LED array used in blue light therapy was created and validated. To create a more uniform light distribution for use on the skin, a diffuser layer composed of silicone and hollow glass microspheres was added between the LED array and the skin surface in the model. This layer was optimized to maximize uniformity while minimizing irradiance loss. Flexible diffusers were fabricated to validate the model with the LED array source. A 1-2 mm thick diffuser layer with hollow glass microsphere volume fraction of 5-10% was determined to provide sufficient diffusion while maintaining an average irradiance >45 mW/cm^2, the minimum irradiance required for blue light inactivation of bacteria. This work is translatable to other phototherapy applications requiring uniform light irradiance from a light source placed near or on the skin.

DEDICATION

I dedicate this thesis to my late father, Frenkel ter Hofstede.

ACKNOWLEDGMENTS

I would like to thank my committee chair Dr. Kristen Maitland, and my committee members, Dr. Limei Tian and Dr. Christi Madsen for their continued guidance and support throughout this research.

I would also like to acknowledge my friends and colleagues at Texas A&M who have also supported me throughout my time here in College Station. In addition, I extend my thanks to Camella Carlson, an undergraduate student who worked with me at the beginning of this project.

Finally, I would like to thank my friends and family for their endless encouragement.

CONTRIBUTORS AND FUNDING SOURCES

Contributors

This work was supported by a thesis committee consisting of Professor Kristen C. Maitland and Professor Limei Tian of the Department of Biomedical Engineering and Professor Christi K. Madsen of the Department of Electrical & Computer Engineering.

The concentric sphere modeling code used in Chapter III was written by Madeleine Durkee and modified by Blanche ter Hofstede.

All other work conducted for the thesis was completed by the student independently.

Funding Sources

Graduate study was supported by the Graduate Diversity Excellence Fellowship from Texas A&M University.

NOMENCLATURE

CCD	charge-coupled device
FDA	Food and Drug Administration
FWHM	full-width half-max
g	anisotropy
HGM	hollow glass microspheres
IR	infrared
LED	light emitting diodes
μ_s	scattering coefficient
μ_s'	reduced scattering coefficient
ND	neutral density
NIR	near infrared
OLED	organic light emitting diode
PCB	printed circuit board
PDT	photodynamic therapy
PDMS	polydimethylsiloxane
PS	photosensitizer
ROI	region of interest
ROS	reactive oxygen species
UV	ultraviolet

TABLE OF CONTENTS

Page

LIST OF FIGURES

FIGURE Page

LIST OF TABLES

TABLE Page

1. INTRODUCTION

1.1 Introduction to phototherapy

Phototherapy is the use of ultraviolet (UV), visible, or near-infrared (NIR) light based on non-thermic tissue reactions that can be applied to a broad range of clinical applications [2, 3]. The wavelength used is determined by the application based on target chromophore and penetration depth. For example, phototherapy has been demonstrated to treat skin conditions such as acne vulgaris, rosacea, eczema, and psoriasis using blue or red wavelengths [3, 4]; shown efficacy in promoting wound healing for diabetic ulcers using red, near-infrared, and blue light [5]; and has long been used to treat neonatal jaundice [6]. In addition, blue light therapy has attracted increasing attention because of its inherent ability to inactivate bacteria, viruses, and fungi with or without the need for a photosensitizer (PS). Photodynamic therapy (PDT), a type of phototherapy, requires an endogenous PS in the tissue or exogeneous PS to be applied to tissue to target cells such as tumor cells [5]. In this work, we are focused on optimizing an LED array using blue wavelengths with a center wavelength of 405 nm for the use of bacterial inactivation. More broadly, the work done here can be applied to a variety of different wavelengths used in phototherapy.

*

1.2 Current light sources in phototherapy

Traditionally, light for phototherapy and PDT has been administered in a clinical environment using lasers and bulky filtered lamp systems [7, 8]. Lasers and laser diodes are the most widely used light sources, that provide high-powered and coherent illumination; however, they are expensive, require specialized safety equipment and training, and are not highly portable [9]. In addition, lasers are not ideal for applications that require large and dispersed illumination areas such as wound healing [10]. Filtered lamps, on the other hand, deliver fairly uniform, wide-field

*Portions reprinted with permission from "Modeling and optimization of immersion medium for phototherapeutic light-emitting diode array for uniform light distribution" by ter Hofstede, Blanche, Glowczwski, Alan, Lovelady, April, Maitland, Kristen C., 2021. Proc. SPIE 11633, Design and Quality for Biomedical Technologies XIV, 116330C, Copyright 2021 by International Society for Optics and Photonics.

illumination over the treatment area, but their utilization has been limited to dermatological applications, and they produce excessive heat [11].

LEDs have been growing in popularity for use in phototherapy and PDT due to their low-cost design, durability, and high efficiencies. Compared to lasers, LEDs are very inexpensive, and new generation LEDs have increasingly narrower wavebands. Although they are not completely monochromatic like lasers and laser diodes, they are quasi-monochromatic making them useful for phototherapy. Additionally, LEDs have been shown to be as effective as lasers and filtered lamps in phototherapeutic applications such as treating jaundice and inactivating bacteria [4, 7]. Furthermore, LEDs allow for greater versatility over other light sources because they can be assembled into arrays using multiple wavelengths for multiple phototherapeutic applications and different configurations of LED placement allowing for multiple geometries [12]. LEDs are configured into arrays of various patterns and wavelengths and attached via an articulated arm so that the device can be placed over the patient.

1.3 Current LED phototherapy devices

There are numerous LED array devices on the market today for therapies such as acne treatment and wound healing. For example, the Omnilux Led phototherapy system found in dermatology offices are rigid LED array devices designed to conform to the face with only one degree of freedom. Features such as the nose are not taken into account and therefore may receive more irradiance than other portions of the face. In addition, because the device is irradiating from a varying distance and the patients' facial features vary in geometry, the dosimetry is difficult to measure because there is no fixed distance. These devices use LED arrays on rigid, non-conforming structures resulting in reduced patient comfort and may interfere with hospital workflow [7].

GE Healthcare has a variety of LED phototherapeutic devices focused on treating hyperbilirubinemia in infants. The BiliSoft 2.0 Phototherapy System, an alternative to the overhead lighting, is a flexible fiber-optic fabric pad with blue LEDs with a peak wavelength of 445-470 nm and an irradiance of up to 49 μW cm^{-2} nm^{-1} (22 mW cm^{-2} at 450 nm). However, this irradiance is measured without the fabric covering and therefore the actual power on the skin is attenuated by the

fabric placed over the light [13].

In addition, acne light devices that utilize red and blue LEDs exist such as illuMask (La Lumiere, LLC) and Omnilux Clear-U that have all been cleared by the Food and Drug Administration (FDA). While many of the phototherapeutic devices on the market are handheld devices where the user must hold the LED device over the affected area, the illuMask is a plastic, rigid mask with LEDs embedded in the mask that utilizes filtered goggles to protect the user's eyes. It has been shown to effectively reduce mild-to-moderate acne in a 12-week randomized, controlled trial [14] while at the same time allows for more consistent dosing as opposed to the handheld systems. The rigidity of the system still is a limitation due to the varying facial geometries. Overall, these current phototherapeutic devices either lack the irradiance required for the inactivation of microbes or are rigid devices that are not easily incorporated into the clinical workflow.

1.4 Flexible LED array bandage

With the use of flexible printed circuit boards (PCB), LED arrays can be assembled into flexible bandages allowing for placement on the patient's skin, replacing the bulky lamp systems currently in use and thus increasing patient comfort. Not only can this be easily incorporated into the hospital workflow because it does not require a trained professional such as in laser therapy, and the patient is also not as restricted as with the overhead lighting. This also allows for more effective dosimetry of the light due to the increased conformability of the device [15]. Depending on where the bandage is placed, the patient is not required to sit still to ensure the treatment is effective.

However, by bringing the LEDs closer to the skin, areas of very concentrated light, referred to here as hot spots, are created. This is not desirable in phototherapy where uniform irradiance is desired to most effectively inactivate target cells [2]. To increase irradiance uniformity, previous groups in light engineering have worked on methods such as optimizing the LED arrangement of the arrays themselves for more uniform illumination [16] or creating customized freeform LED lenses [17]. However, these methods either are not sufficient when the light source is placed close to the skin or require a high degree of customization that is not feasible for applications where the use of low-cost, commercially available LEDs is desired. In addition, organic LEDs (OLED) for

PDT have also been investigated to create a uniform distribution for a wearable device. OLEDs are prone to the burn-in phenomenon and have shorter lifetimes than LEDs, especially when run at a high luminance for extended periods of time. The irradiance delivered onto the skin by the OLEDs is not sufficient in inactivating bacteria or other microbes that severely limits their use for this application [18].

Diffuser panels have been used to create a more uniform distribution from the focused light emitted from the LEDs in overhead lighting. These panels are rigid but the same concept of using a diffuser to spread the incoming light can be implemented to a flexible LED array [7]. We aim to model and optimize a flexible, diffusing material composed of soda-lime borosilicate glass microbubbles fixed in a matrix of polydimethylsiloxane (PDMS) to be placed in between the LED array (Figure 1.1) and the skin. This composite material will scatter light emitted from an LED array creating a more uniform illumination without reducing the irradiance required for phototherapy.

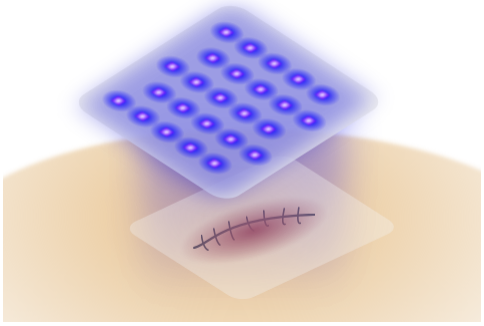

Figure 1.1: Flexible LED array with peak wavelength at 405 nm designed for prevention of bacterial infections at surgical sites.

1.5 Thesis Overview

In this work, a previously fabricated flexible blue LED array was modeled in the optical simulation software LightTools, and subsequently, using different materials as a medium between the

LED array and the patient's skin, the distribution of the emitted light was optimized to create a uniform illumination without significantly reducing the irradiance on the patient's skin. The model was validated experimentally at multiple stages to ensure accuracy allowing for future modifications. Furthermore, the model can be used in various other phototherapy and lighting applications with a variety of wavelengths to assess the effectiveness of the light distribution administered by simply adjusting the LED array's properties such as geometry and wavelength.

2. BACKGROUND

2.1 Mechanism of phototherapy

The effectiveness of phototherapy requires both appropriate wavelengths for targeting chromophores and penetration depth in addition to adequate irradiance depending on the therapeutic application. Longer wavelengths such as red and NIR penetrate deeper into the tissue because the absorption and scattering coefficients of chromophores in tissue are highly wavelength dependent. Blue light, however, penetrates tissue with an intensity decrease of approximately 63% at 1 mm while NIR can penetrate up to 5 mm [19]. Figure 2.1 shows the penetration depths in human tissue for UV through NIR light .

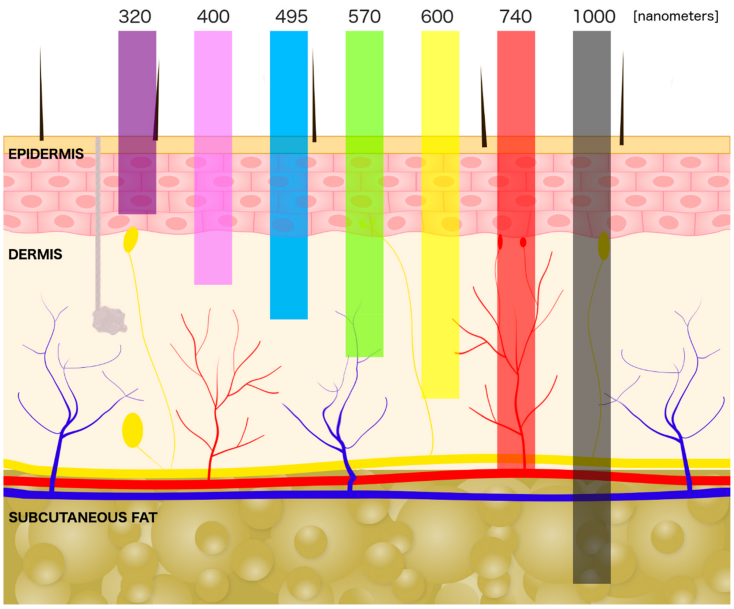

Figure 2.1: Diagram of light of different wavelengths (UV-NIR) penetration depths in human tissue [1].

Red (~600 - 750 nm) and NIR (~750 - 1100 nm) light have been shown to promote wound healing [20] and pain management [21] due to the profound effect on macrophages, fibroblasts, and

epidermal keratinocytes that are critical cells in the inflammatory, proliferative, and remodeling stages of wound healing. It is theorized that red light targets cytochrome c oxidase (CCO), the respiratory chain of the fibroblasts' mitochondrion [22, 20] that converts molecular oxygen to water during the electron transfer redox chain; whereas, NIR affects cell proliferation [23]. Research utilizing green light (495 – 570 nm) recently has shown improvements in cellulite appearance [24] and inflammatory effects [25].

In addition, the blue portion of the visible spectrum (400 – 500 nm) has been shown to have anti-inflammatory properties in superficial tissue [26], promote wound healing, and exhibit inflammatory effects with the potential to inactive bacteria such as acne vulgaris [27], fungus, and viruses [5]. Blue wavelengths are shown to excite flavins and flavoproteins that leads to the catalyzation of reduction of oxygen to superoxide producing reactive oxygen species (ROS). Studies have shown that blue light promotes opsin signaling; however, the complete signaling pathway is not completely understood [28]. Also, blue light therapy is considered an endogenous PDT because it uses endogenous porphyrins, a group of heterocyclic organic compounds complexed to proteins such as haemoglobin and cytochrome. Propionibacterium acnes contains endogenous porphyrins protoporphyrin IX and coproporphyrin III that have a strong absorption peak at 415 nm at which ROS will be generated and destroyed via apoptosis without harming mammalian cells [29].

2.2 Radiometry and photomedicine dose reporting

Radiometry is the area of optics concerned with measuring the light radiation's power in space as opposed to photometry that involves the study of how the human eye perceives light. In radiometry, the flux of all electromagnetic radiation in the optical spectrum (UV, visible light, IR) is measured using units such as power (Watts), irradiance (Watts m^{-2}), and radiance (Watts m^2 sr^{-1}), whereas in photometry, light is weighted by the human eye's spectral response. The standard unit of flux is the lumen and includes functions such as color temperature analysis and illuminance [30]. Because this application does not involve how our eyes perceive light and needs the absolute flux of light, radiometric measurements are utilized in this work. In addition, LED specifications are typically reported in photometry units because of their use in lighting applications.

Power is the measurement of photons flux per second where 1 Watt is equal to 1 Joule per second. This can be measured using an optical power meter that takes the average over a period of time using a photodiode. Irradiance is the measurement of power over an area (power density). This is one of the critical values to report in phototherapy in clinical and laboratory studies. Often only the dose of light (Joules or J/cm^2) are published based on the now disproven Bunsen-Roscoe law of reciprocity, or the third law of photobiology [31]. However, this law has been disproven by Lanzafame et al. who showed that by radiating a murine pressure ulcer model with increasing irradiance and decreasing treatment time, although the energy density was constant, different effects were produced [32]. Other important measurements include the pulse wave velocity, length of dose, beam area at skin or culture surface, and anatomical location [31].

2.3 Light-emitting diodes

LEDs are light sources that produce non-coherent light from a semiconductor diode that converts electrical energy into light energy. The p-n junction at the diode die emits light when conduction electrons in the forward current fall into valence band holes, releasing photons in the process as shown in Figure 2.2. The color emitted by the LED is determined by the semiconductor material and impurities used to form the p-n junction [33].

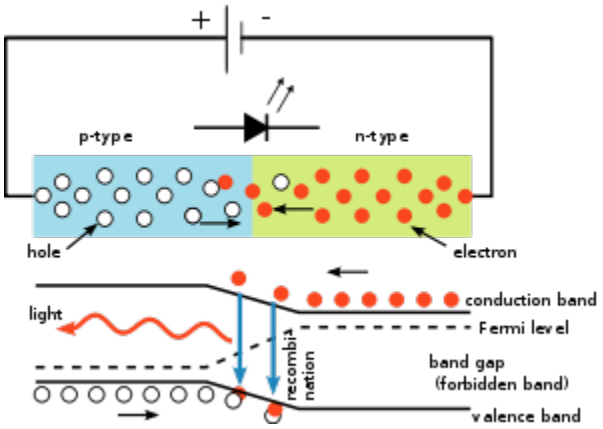

Figure 2.2: Schematic of LED p-n junction at diode die. As forward current flows across the junction, electrons in the conduction band fill electron holes in valence band releasing photons in the process.

The power output and efficiency (radiated power output/electrical power inputted) have increased over the last two decades where now LEDs can output greater than 1 W starting in 1999. In addition to efficiency, LEDs also have a long lifetime that is measured by when the LED's intensity decreases to 70% of its original intensity. The average lifetime specification of high-power LEDs is about 50,000 hours which is 2-3 times better than traditional fluorescent or high-intensity discharge lamps [34].

Typically, LEDs are composed of a diode, reflector, and silicone lens. To increase photon efficiency, the reflector, which is part of the chip cathode, aids in ensuring that the photons generated by the chip cathode are reflected out of the envelope tip. The lens helps determine the angular intensity distribution of the output light. Typically, this value ranges from 60-120° depending on the application. Current generation LEDs can have a smaller angle of divergence for a more focused beam [9]. LED packages come in different types such as chip style and surface mounted LEDs for different applications. I will be focusing on surface source LEDs that are used in the previously designed LED array device described in this work.

In order to model LEDs, different levels of complexity can be used depending on the application. As a first-order model, a simple point source can be used with spectral information provided by the data sheet. This can give a general idea of flux of the LED [35]. For higher order models, a surface source using an apodization file that consists of the angular intensity data provided by the LED data sheet can be modeled. This method assumes that the angular distribution and spatial distributions are independent. The most complex and accurate is modeling a 3D geometrical model of the LED including the diode, reflector, and lens. This can be time consuming however because LED manufacturers usually do not provide all the required information. Therefore, the geometric and optical properties must be adjusted until the angular intensity distribution matches the data sheet. Some manufacturers provide the mechanical model and ray data that can be imported into optical simulation software such as LightTools [36, 35]; however, this was not available for the current LED used in the LED array.

2.4 Monte Carlo modeling

Monte Carlo simulation of light transport illustrated in Figure 2.3 is a stochastic method for modeling light propagation. This method adapted by Jacques et al. in 1995 has been used and adapted extensively in tissue optics for therapeutic applications such as evaluating angular radiance of a dye laser in human prostate for PDT [37, 38].

In this well-defined method, photon packets are launched individually into the medium and moved through with a step size determined using a probability density function. With each step, the photon packet experiences scattering and absorption events where the photon will be deflected at an angle, and its weight (intensity) is decreased determined by the probability density function and the material's optical properties. If the photon packet's weight is below a set threshold and does not survive a roulette step based on a random number generator, the photon will be terminated. Otherwise, the photon will continue stepping through the material until it does not survive the roulette step. If the photon hits a boundary, it will either reflect or transmit to the next boundary. After a sufficiently large number of photons have propagated through the material, the simulation should accurately represent the solution of the light transport problem where measurements like transmittance, reflectance, and radiance are computed [39].

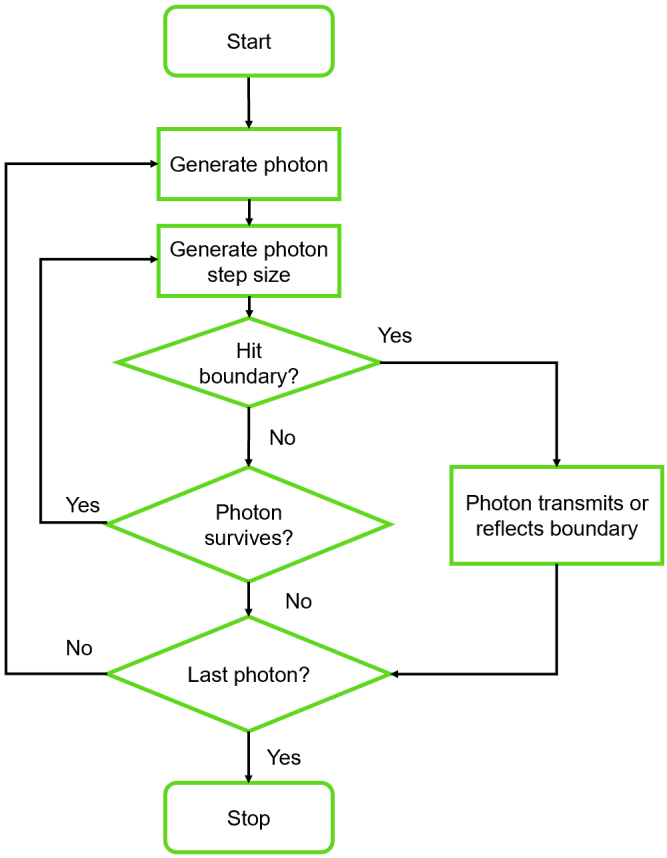

Figure 2.3: Flow diagram of Monte Carlo model decision process of photon propagation including absorption, scattering and reflection events. Process is repeated until all photons have reached end of their lifetime or traveled through material.

2.5 Light Diffusers

Light diffusers have long been used in optical design to create uniformity by decreasing the difference between high and low brightness. Light diffusion occurs in optically mixed environments where the index of refraction fluctuates irregularly [40]. Fillers such as organic and inorganic particles known as light-diffusing additives are added to create this effect. Many overhead lighting systems in recent years have transitioned from incandescent light bulbs to more energy-efficient LEDs with the help of diffusers that scatter the light to create illumination similar to that of a traditional light bulb. Diffusers are also used in cell phones to evenly illuminate the back screen

designed precisely to decrease wear on the user's eyes [41].

Hollow glass microspheres (HGMs) are used as an additive in polymeric compositions to create scattering of light due to their high stability and low density [42]. In addition to light scattering, HGMs have been shown to have thermal insulating properties, which is advantageous for the application present here because high power LEDs do produce a significant amount of heat especially when applied to the skin for extended periods [43]. Sodium-lime borosilicate hollow glass microbubbles were utilized that have a diameter (30 - 90 μm) greater than the wavelength of the incident light (405 nm). Therefore, the behavior of light can be described by Mie scattering, that uses solutions to Maxwell's equations for interaction of electromagnetic waves with particles. Mie scattering of multi-layer concentric spheres has been previously described by Aden and Kerker [44], where a third Mie equation accounts for the electromagnetic field in the shell dielectric. From the Mie coefficients, the bulk optical properties of the materials can be extracted to find the scattering coefficient (μ_s), anisotropy (g), and reduced scattering coefficients (μ_s') [45, 46].

PDMS is a type of silicone that is flexible and has a low optical loss (< 95%) making it a great candidate for incorporation into a form-fitting device to be placed on the skin. Some types of medical-grade silicone such as Silastic MDX4 (DuPoint) are available that are used in implantable devices previously cleared by the FDA [47].

HGBs can be added to PDMS before curing to create a flexible diffuser that can be incorporated into the LED bandage between the LED array and the skin. The fact that it is form-fitting allows for the bandage to stay flexible while spreading the light to be more uniform. However, there is an issue with power loss through the PDMS and HGBs that needs to be optimized.

2.6 Gaps in literature

Overall the area of phototherapy is not completely understood and lacks in accurate and consistent dosimetry leading to inconsistent results. Flexible LED arrays can be used to create phototherapeutic devices allowing for placement close to or on the skin for more consistent dosimetry. However issues with LEDs creating areas of non-uniform irradiance on the skin have not been addressed. A method of diffusing the light emitting from LED arrays to create a more uniform

light distribution without sacrificing power is needed in phototherapy.

3. OPTICAL SIMULATION OF LED ARRAY DEVICE AND FLEXIBLE LIGHT DIFFUSER

3.1 Materials and Methods

In this chapter, I will discuss the methods utilized to simulate a blue LED array device using the optical simulation software LightTools (Synopsis, Inc.), the LED placement optimization, and the optimization of a medium placed between the LED array and the skin used to create a more uniform irradiance.

3.1.1 Modeling of LED array

A previously designed, flexible LED array shown in Figure 3.1a made up of 51 blue LEDs was modeled using the optical simulation software LightTools that utilized the Monte Carlo method to model photons as they move through free space and various materials. The LEDs (QBHP684E-UV405BS, QT Brightek) have a viewing angle of 120°, a center wavelength of 405 nm, and a full-width half-maximum (FWHM) of 16 nm that was provided by the manufacturer datasheet. Using apodization data, a source model was created where one surface emitted light according to the angular and spectral intensity distributions provided by the datasheet shown in Figure3.1b. It was assumed the LED had a Lambertian intensity distribution.

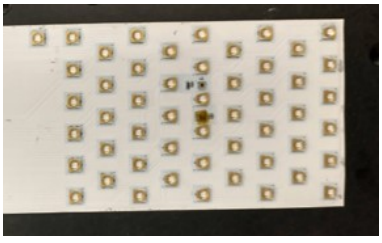

(a)

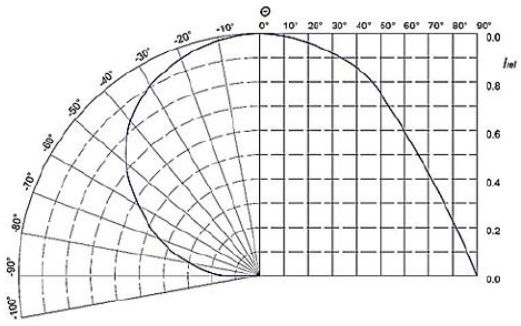

(b)

Figure 3.1: (a) The blue LED array with 51 LEDs powered off used for optical simulation and experimental testing. The LEDs have a peak wavelength of 405 nm and are controlled using a Python graphical user interface. (b) Angular distribution of LED used in LED array.

Once the LED source model was created, the LEDs were arranged into an array using the layout geometry of the device in Figure 3.1a. A PCB backing of aluminum was also modeled to account for any reflection off this surface.

3.1.2 Modeling of intermediate medium

To create a more uniform distribution of light using the existing LED array, a medium can be placed between the LED array and the skin. First, the geometrical properties such as thickness and material were optimized using LightTools. Three immersion materials were simulated: air (n = 1.0), PDMS (n = 1.43, Sylgard 184, Dow Corning), and water (n = 1.33). For the water medium, a thin layer of polyethylene coating was added on either side to model a bag to contain the water. The irradiance incident on the tissue over an area of 100 X 60 mm^2 was simulated and compared for the three materials of varying thicknesses.

In addition, uniformity over a region of interest (ROI) (60 x 24 mm^2) was compared for varying medium thicknesses ranging from 1 mm to 15 mm. This ROI was chosen because complete uniformity over the entire array is unlikely and for phototherapeutic applications such as wound healing, the ROI is the area of the wound at the center of the LED array. The uniformity was measured by comparing the standard deviation of the irradiance in this region.

3.1.3 Modeling and optimization of diffuser

Following the geometrical and material simulations, a flexible diffuser was modeled in LightTools by distributing soda-lime borosilicate HGMs with varying volume fractions to a matrix of PDMS. Mie scattering for concentric spheres was used for the simulation of the bulk material for this diffuser. MATLAB code developed by Durkee et al. [45] was used to find the anisotropy factor (g) and the scattering coefficient (μ_s) using the Mie equations for two-layer concentric sphere model developed by Aden and Kerker in 1951 [44] that calculates the Mie scattering coefficients. The radius of the spheres ranges from 30 - 90 μm with a mean diameter of 60 μm and an estimated shell thickness of 2-5 μm, based on the density. μ_s and g were found for wavelength range 350 nm - 450 nm assuming the HGMs were uniformly 60 μm in diameter with a shell thickness of 3 μm and

a refractive index of 1.64 at 405 nm embedded in PDMS (n = 1.43). Then, the Henyey-Greenstein phase function was used to find the angle of scattering in LightTools.

To optimize the diffusion of light at the skin, the volume fraction of the HGBs was varied from 0-40% by finding μ_s and g for each volume fraction. The volume fraction is positively correlated to the μ_s and therefore, adding more HGBs to the composite material increases scattering. The uniformity and irradiance at the ROI for mediums of thickness 1 mm, 2.5 mm, and 5 mm were found and compared.

3.2 Simulation results

The results are presented here for the simulation in LightTools of both the LED array and intermediate material. All results were found using $1x10^7$ photons and run on a personal desktop computer (8-core AMD FX(tm)-9590 processor, 4.70 GHz, 32 GB RAM).

3.2.1 LED array model

The LED surface source modeled is shown in Figure 3.2a where one surface of the volume emits light corresponding to the angular distribution provided by the datasheet as shown in Figure 3.2a. The spectral distribution with a peak wavelength at 405 nm and a FWHM of 16 nm are shown in Figure 3.2b. The total output power of the individual LED was 0.07 W that was calibrated with experimental results discussed in the following chapter.

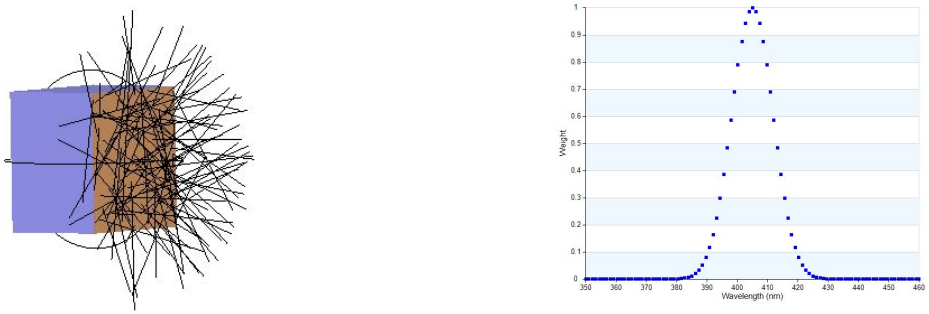

(a) (b)

Figure 3.2: Simulation results of (a) surface model of individual LED with sample ray tracing and (b) spectral distribution of each LED with a peak wavelength at 405 nm and a FWHM of 16 nm.

The angular distribution simulated using the surface source is compared to the angular distribution provided by the manufacturer in Figure 3.3a and 3.3b.

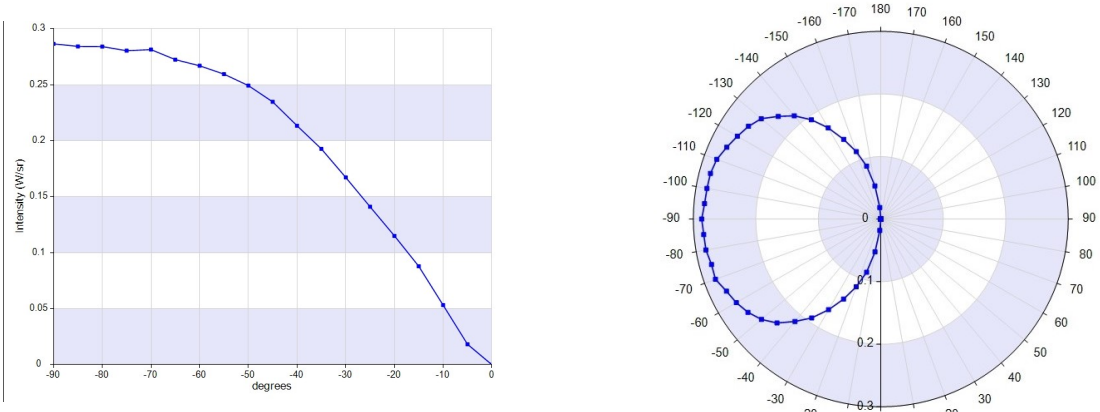

(a) (b)

Figure 3.3: Simulation of LED surface source's angular distribution in (a) Cartesian and (b) polar coordinates.

The LED array was then modeled after a previously manufactured array as shown in Figure 3.4 using 50 LEDs to simplify uniformity measurements. The average output irradiance for the receiver 1 mm away at the 60 X 24 mm^2 ROI of the LED array was 90.4 mW/cm^2 with an error of less than 5%.

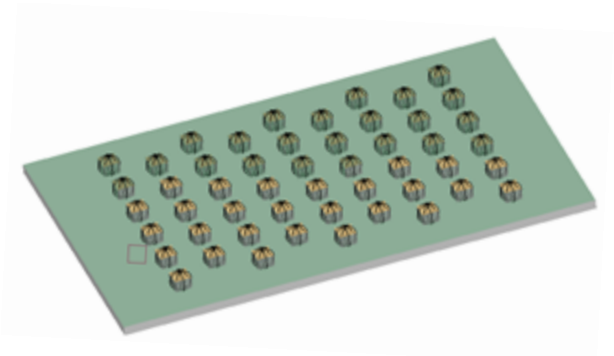

Figure 3.4: LED array modeled using PCB backing simulated in LightTools using surface sources.

The irradiance distribution output with the receiver 0.5 mm away is shown in Figure 3.5 with horizontal and vertical line plots through the middle of the LED array. The LED irradiance hot

spots can be seen in the simulation because the LEDs are close to the receiver. The goal of this work is to remove these hot spots and redistribute the light in the following sections.

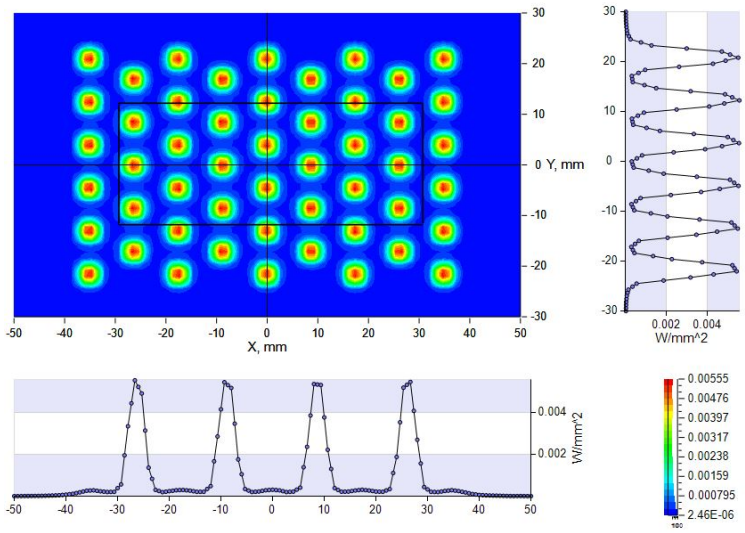

Figure 3.5: Example simulation irradiance distribution of LED array 0.5 mm away from receiver (skin) in air. ROI is indicated by black rectangle where irradiance and uniformity measurements were calculated. Horizontal and vertical line plots through middle of LED array show the lack of uniformity of the irradiance. Units are in W/mm^2

3.2.2 Immersion medium results

A medium was placed between the LED array and the receiver (skin). The effects of the geometrical properties of the medium were compared by changing the thickness and material. The thicknesses ranged from 1 mm - 15 mm and the materials for the medium were PDMS and a water pack comprised of water and a layer of polyethylene to simulate a plastic bag. These two materials were compared to air to assess the change in uniformity and irradiance. Figure 3.6 and 3.7 show the comparison of the three materials (air, water, and PDMS) for the varying thicknesses. As the thickness increases, the uniformity over the region increases; however, the average irradiance decreases. This is due to the absorption of light as it interacts with the material. In the case of air, the light is absorbed and scattered by particles in the air such as water but there is no focusing

of the light towards the region of interest and instead light is lost to areas outside the region of interest. For PDMS and the water pack, the light refracts at the interface between air and the material causing refraction, redirecting the light to the ROI.

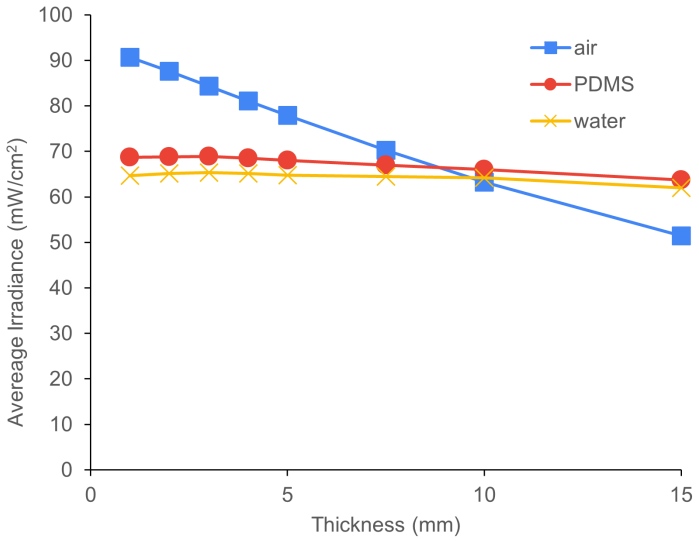

Figure 3.6: The simulated average irradiance incident in ROI (60 X 24 mm^2) of LED for silicone, a water bag, and air of thicknesses ranging from 1 mm - 15 mm.

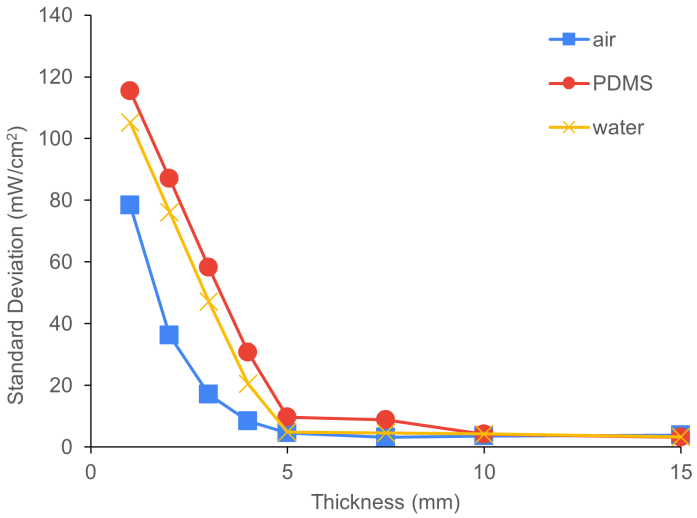

Figure 3.7: The simulated change in irradiance standard deviation as the thickness of three materials (silicone, a water bag, and air) increases from 1 mm to 15 mm.

PDMS proved to be the most efficient at maintaining power on the skin receiver that can be attributed to its low optical power loss. A comparison of the spatial irradiance of PDMS from 1 mm and 10 mm is shown in Figure 3.7 where as the thickness increased, the uniformity increased. The water pack was comparable in uniformity; however, the use of silicone is more practical compared to a water pack for clinical applications where implementing the technology into the hospital workflow is critical for product adoption.

3.2.3 Optimal light diffusing composite

HGM of diameter 30 - 90 μm were added to the material to scatter light due to the change in the index of refraction of the material and the air within the beads governed by Mie scattering. The average scattering coefficient, anisotropy, and reduced scattering coefficients are shown below in Table 3.1 over wavelengths 350 nm - 450 nm. As the volume fraction increases, the scattering of the bulk material increases.

Table 3.1: Calculated bulk optical properties averaged over 350 - 450 nm wavelengths for 1% - 40% volume fraction of HGMs.

Volume Fraction (%)	μ_s [cm^{-1}]	g	μ_s' [cm^{-1}]
1	5.0533	0.7914	1.0533
5	25.2667	0.7914	5.2667
10	50.5334	0.7914	9.9515
20	101.0668	0.7914	21.067
30	151.6001	0.7914	31.6005
40	202.1335	0.7914	42.1339

Next, the volume fraction was optimized for the medium using 60 μm diameter HGBs. In addition to scattering the light, the HGBs also absorb energy. Therefore, the optimal volume fraction of HGBs was found to maximize light scattering and minimize absorption. Using thicknesses of 1 mm, 2.5 mm, and 5 mm, the volume fraction of the HGBs was varied from 0-40%. An example of the geometrical model for a 5 mm diffuser with a volume fraction of 40% in Figure 3.8 illustrates the scattering of light in the medium.

Figure 3.8: Example simulation of rays through PDMS composite material of thickness of 5 mm with 40% volume fraction HGMs.

The results for the 1-5 mm thick medium are shown in Figure 3.9a and 3.9b. The absorption as the composite material for volume fractions greater than 1% increased was too significant and the irradiance on the skin after 5 mm converged to an average zero mW/cm^2 in the ROI. As the volume fraction increases, the uniformity is expected to increase as the light emitted from the LED array scatters the light through the composite material. Figure 3.9b shows a decreasing standard deviation of the irradiance as the volume fraction of HGMs increases which indicates an increase in uniformity. However, the irradiance as shown in Figure 3.9a decreases below 45 mw/cm^2 as the volume fraction increases. From these results, I found that a diffuser of 1 mm with a volume fraction of between 5-10% was ideal for creating a uniform light distribution without decreasing the power below 45 mW/cm^2.

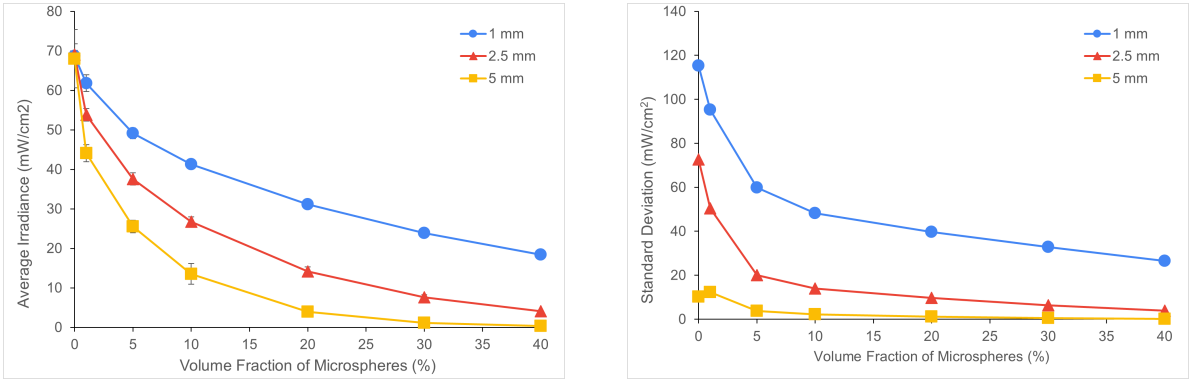

(a) Irradiance (b) Standard Deviation

Figure 3.9: Simulation results of (a) average irradiance and (b) standard deviation over ROI (60 mm X 24 mm) as the volume fraction of HGM increased from 0% to 40%. Thicknesses of medium ranged from 1 mm to 5 mm.

4. EXPERIMENTAL VALIDATION AND TESTING

4.1 Materials and Methods

This section describes the methods used to validate the optical modeling of the LED array and diffusing silicone material reported in Chapter III using both spatial and irradiance measurements.

4.1.1 LED array validation

The final array simulation was verified using a Thorlabs PM100D optical power and energy meter and a Thorlabs S120C sensor to measure the power detected from the LED array where the average irradiance and standard deviation were compared. To find the output of a single LED, the power output was measured at different distances using a power meter and the corresponding setup was simulated in LightTools using a receiver the size of the power meter receiver.

In addition, an optical setup (Figure 4.1) using a charge-coupled device (CCD) camera (Blackfly Monochrome CCD Camera, FLIR), an achromatic doublet lens with focal length of 30 mm (AC254-030-A1, ThorLabs), and absorptive neutral densities filters (ND) (NE-A, Thorlabs) with a total optical density of 0.9 were used to verify the spatial variation of the array using line plots. Both the pixel intensity and irradiance were normalized after confirming the irradiance using the power meter.

4.1.2 Diffuser fabrication and testing

The diffusers were fabricated by embedding soda-lime borosilicate glass microbubbles (Glass Bubbles K16, 3M) in uncured PDMS (Sylgard 184, Dow Corning) with 0-40% microbubbles by volume. The samples were made in a model with a dimension of approximately 12 cm X 8 cm to cover the entire LED array. The samples were cured at 65°C for 95 minutes and let sit for 24 hours before removing from the mold. 3 samples of each volume fraction were fabricated and the averages of the measurements were averaged together. The diffusers' thicknesses were measured at 3 different points and placed between the LED array and the receiver as shown in Figure 4.1 for testing using a power meter and CCD camera optical setup for spatial information. These were

compared to the simulation results found in the previous chapter.

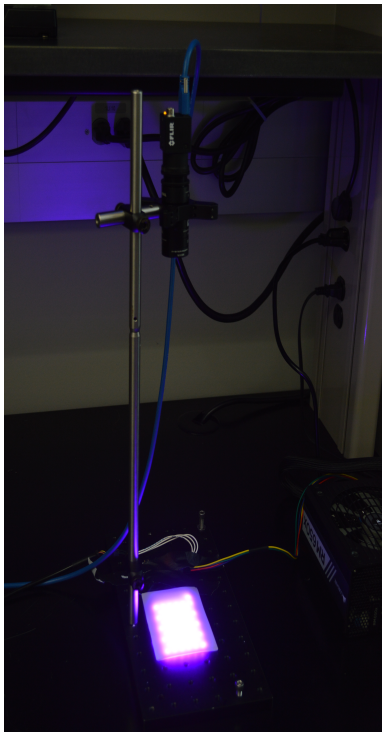

Figure 4.1: Optical set up consisting of CCD camera, doublet lens, and ND filters (OD = 0.9) used to measure spatial variation of irradiance. LED array was approximately 40 cm away from CCD camera.

4.2 Results

The results from the LED array and silicone diffuser medium are presented in this section. This ensures the simulations done in Chapter 3 are accurate and can be used for future simulations for further optimizations.

4.2.1 LED array validation

A single LED was measured using a power meter and it was found that each LED had an average emittance of 0.07 W. Images of the LED array taken using the CCD camera and LightTools simulation results are shown below in Figure 4.2. The line plots show similar peaks at the hot spots of the LEDs that was used to measure the change in uniformity as the difference in the base line and the peaks decrease.

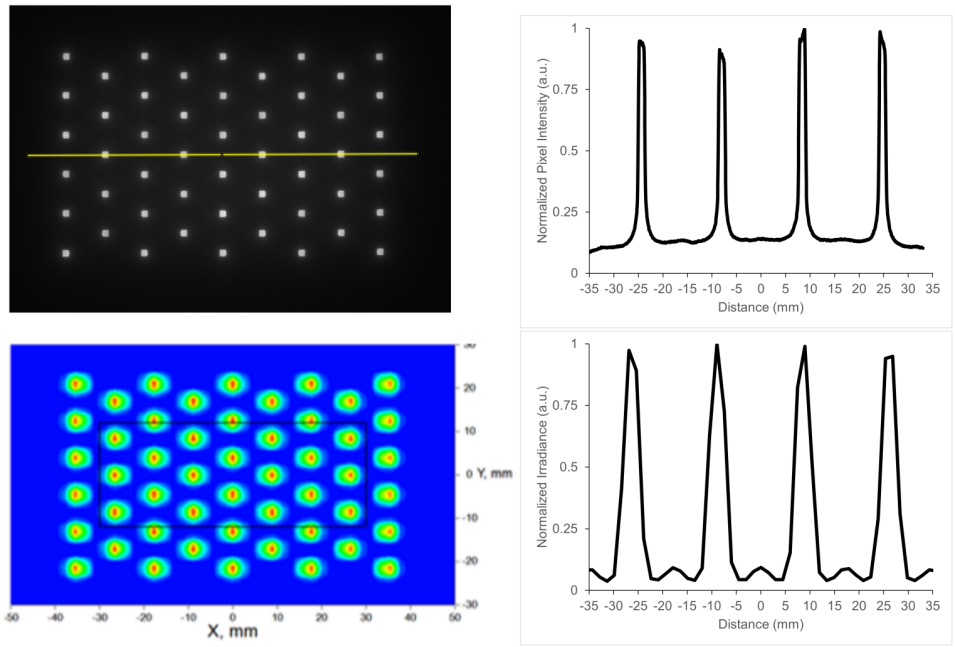

Figure 4.2: Comparison of (a) simulation line plot to (b) RAW image taken using optical system.

4.2.2 Diffuser experimental results and simulation validation

Next, the flexible diffuser composed of HGMs in PDMS of varying volume fractions was created and tested. The thicknesses of the diffusers are shown in Figure 4.3a. The irradiance at the ROI was measured and images were acquired using the imaging setup. Results for the irradiance measurements are shown below in Figure 4.3b. As expected, as the volume fraction increases, the uniformity increases as indicated by the decreasing standard deviation. However, the irradiance decreases with an increase in volume fraction of HGMs. For our blue light application, using the current power output of the LEDs, a volume fraction greater than 10% for a mean thickness of 1.5 mm is not desired given the requirement of at least 45 mW/cm^2.

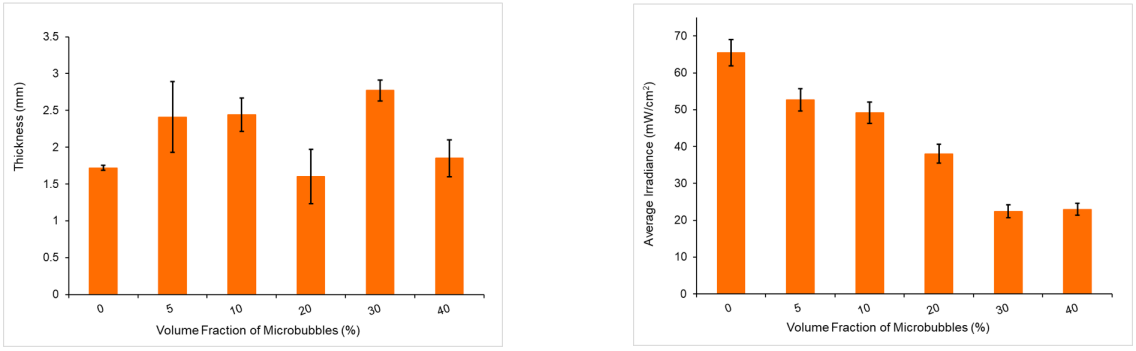

(a) Thickness of diffusers

(b) Irradiance

Figure 4.3: Experimental results of (a) average irradiance (mW/cm^2) and (b) standard deviation (mW/cm^2) found using power meter over ROI. Thicknesses of medium varied from 1.27 mm to 2.36 mm.

The results of the simulation and experimental LED arrays are compared below to show the change in uniformity for diffusers with an average thickness of 2.01 mm with a range of 1.35 mm - 2.55 mm. As in the simulation, as the volume fraction increases, the uniformity at the ROI increases while the irradiance incident on the skin decreases. The irradiance as the volume fraction increases for both the simulation (blue) and experimental (grey) results are shown in Figure 4.4 below.

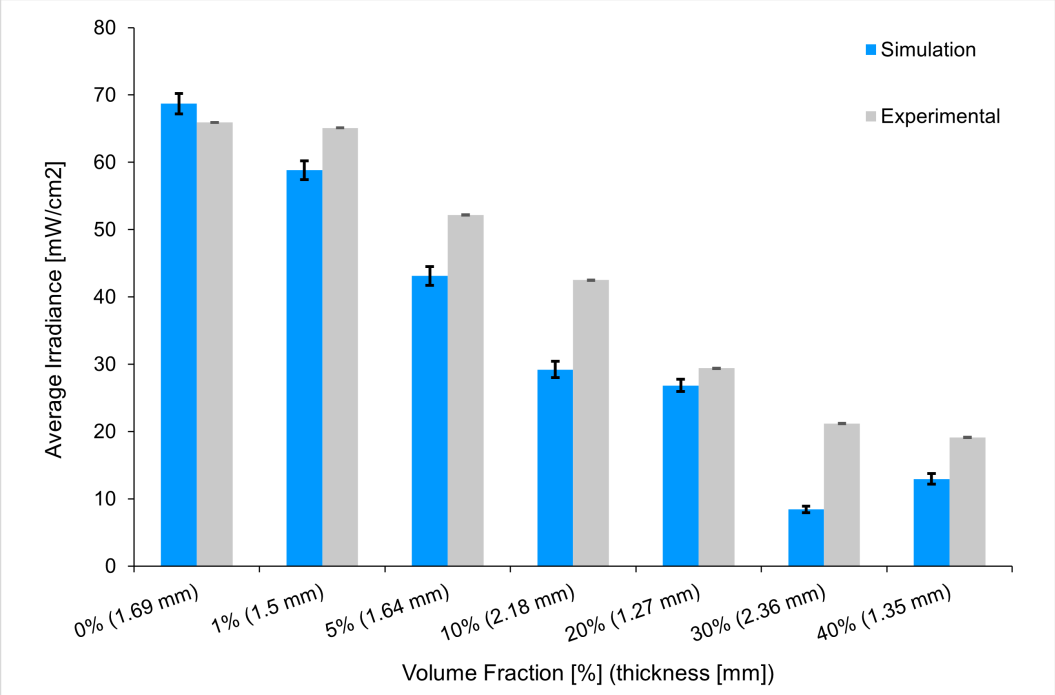

Figure 4.4: Comparison of experimental and simulation results of average irradiance (mW/cm^2) after light emitted from LED array passes through diffusers of volume fraction HGMs with varying thicknesses ranging from 1.27 mm - 2.36 mm.

As the volume fraction increases, the simulation's percent error increases and that can be attributed to a variety of factors. The simplification of the LED light source could have affected the accuracy since the LEDs are near the interface of the diffuser. When testing experimentally, the LEDs were not perfectly incident on the PDMS diffuser, and therefore, there may be slight variations in the results. In addition, the thickness of the medium varied over one diffuser that can have a large impact on the irradiance output. The HGBs was assumed to have an average diameter of 60 μm and be uniformity distributed in the PDMS matrix in the simulation. However, experimentally this can differ from diffuser to diffuser.

Lastly, the spatial irradiance of the diffuser was found using the CCD camera images after background subtraction. Figure 4.5 shows the images for a 0%, 5%, and 20% volume fraction diffuser with its corresponding normalized line plot. It can be seen that the line plot peaks spread out indicating a more diffuse light distribution on the skin. However, for the 20% and 40%, although

the line plots are very uniform, the irradiance was significantly reduced from 65 mW/cm^2 to 29.4 mW/cm^2 and 19.1 mW/cm^2, respectively. These results confirmed the simulation's predictions that a diffuser with 5-10% volume fabrication of HGM and a thickness of 1-2 mm improves uniformity without reducing the average irradiance below 45 mW/cm^2 that is required for the application of inactivating bacteria for blue light therapy.

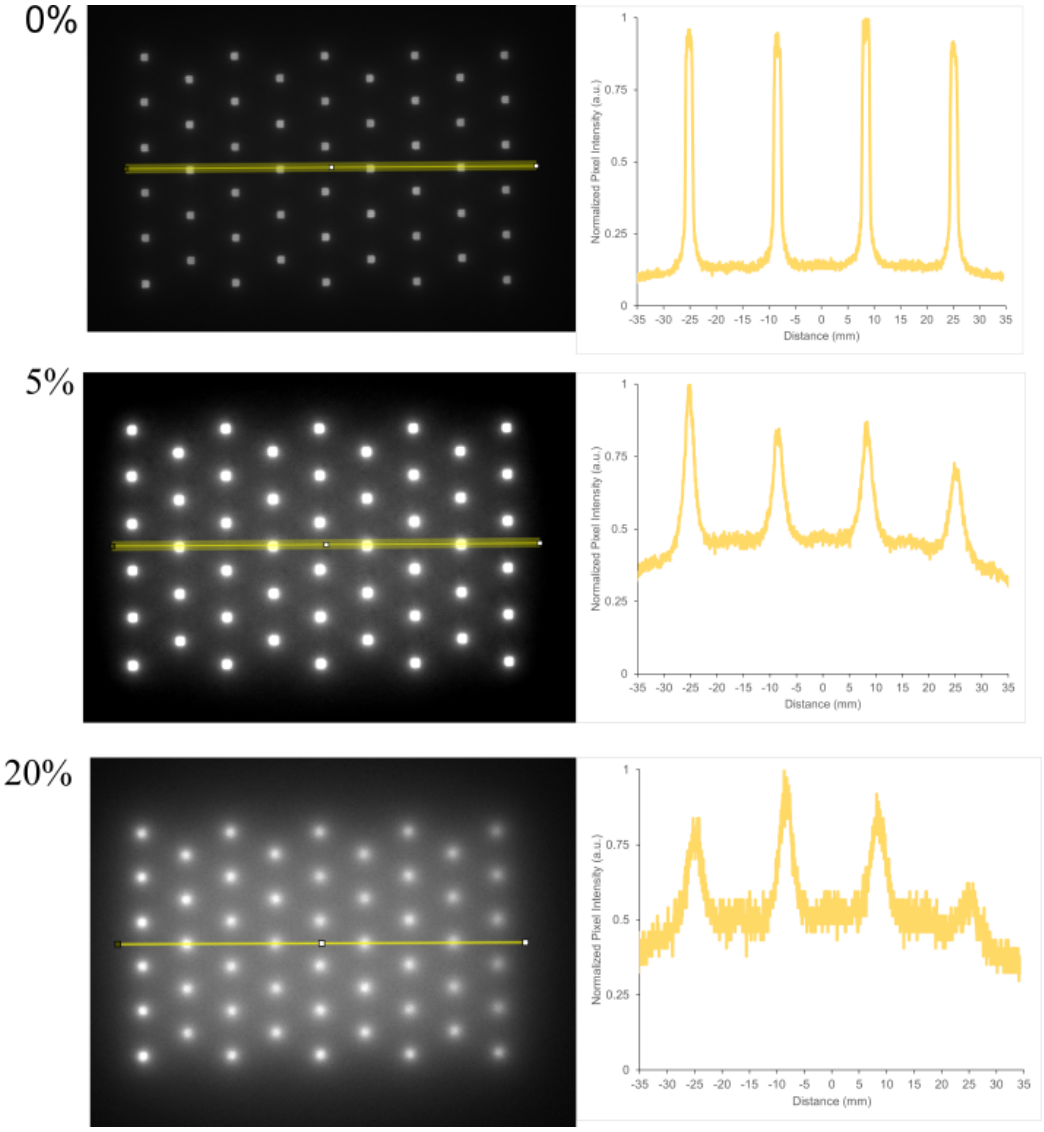

Figure 4.5: Monochrome images of irradiance distribution and horizontal line plots of normalized pixel values through center of array after light emitted from LED array passes through diffusers with 0%, 5%, and 20%. Image brightness has been adjusted in order to visualize differences in diffusion of light.

5. SUMMARY AND CONCLUSIONS

5.1 Summary

Phototherapy is the use of light for therapeutic applications such as treatment of acne, wound healing, and inactivation of microbes. LEDs have become an attractive alternative to the traditional light sources used in phototherapy such as lasers and filtered light systems due to their higher efficiencies, lower costs, and design flexibility. In addition, LEDs can be arranged on flexible PCB boards in a variety of wavelengths and spatial configurations allowing for more customization in terms of the treatment area on the body and therapeutic application. However, when LEDs are placed close to the skin, hot spots of light are formed that leads to areas on the skin that are not receiving the adequate irradiance required for treatment. Therefore, a method of creating a more uniform light distribution is essential without increasing the number of LEDs required that increases cost, temperature output, and power needed.

In this work, we have modeled and optimized a LED array in LightTools utilizing a peak wavelength of 405 nm for use in blue light therapy, a type of phototherapy, for the inactivation of bacteria. A composite material was modeled and fabricated to be placed between the LED light source and the skin to create a more uniform illuminance distribution on the skin that has been proven to increase the effectiveness of phototherapy. The medium's geometrical and material properties were explored and it was found PDMS was the most practical for clinical adoption due to its low optical loss and flexibility.

To further diffuse the light, scattering HGMs were embedded in PDMS. The volume fraction of the microbubbles was found using optical simulations to optimize the light uniformity without decreasing the irradiance significantly. These simulation results were compared to experimental results and the simulations were found to be relatively accurate in terms of both irradiance on the skin and spatial distribution of light on the skin. It was found that a volume fraction between 5-10% with a thickness of 1-2 mm was optimal for our application of bacterial inactivation using

blue wavelengths with a target irradiance of 45 mW/cm^2.

5.2 Conclusions

Overall, this work was successful at optimizing a diffusing silicone medium for uniform light distribution of light on the skin for phototherapy using optical simulations and validated using experimental methods. Although the percent difference, especially for the higher volume fraction of HGMs, was not ideal, improvements to the optical simulation can be made such as using a geometrical model of the LED. When using the silicone diffuser experimentally, the uniformity increased. Even though blue light was used for the model and experimental results, our work could be applied to other wavelengths for other therapeutic applications in order to achieve uniform illumination close to the skin.

5.3 Future Work

Future plans for this work include improving the model of the LEDs to use geometrical LED sources instead of surface sources using apodization. Although this would be more computationally expensive, it is possible for further simulations. In addition, if another type of LED were used, ray files and mechanical models available on many LED manufacturer's websites can also be used.

The HGMs used have a large distribution of sizes ranging from 30 μm to 90 μm with a mean size of 60 μm. Within this range, the scattering coefficient increases as the radius decreases. This can be used to our advantage by filtering out the larger microbeads so that the diffuser scatters the light more effectively.

In addition, to further expand upon the model, future work can be done to model the effect of the diffuser on the penetration depth into the skin as opposed to just looking at the light distribution on the surface of the skin. This can be tested using optical phantoms and the current optical system could be modified to image the light penetration in tissue of the blue light LED array.

Lastly, because the skin is not a flat receiver like in this work, the geometries of the receivers can be modified to add curvature to model areas where this device would frequently be used such as the arm, hip, and thigh. The curvature of the body affects the distribution of the light and the

diffuser may also help with decreasing the concentrated light due to the curvature even further if optimized.

REFERENCES

[1] A. Cios, M. Ciepielak, L. Szymanski, A. Lewicka, S. Cierniak, W. Stankiewicz, M. Mendrycka, and S. Lewicki, "Effect of Different Wavelengths of Laser Irradiation on the Skin Cells," *International Journal of Molecular Sciences*, vol. 22, p. 2437, 2 2021.

[2] S. Y. Lee, C. E. You, and M. Y. Park, "Blue and red light combination LED phototherapy for acne vulgaris in patients with skin phototype IV," *Lasers in Surgery and Medicine*, vol. 39, no. 2, pp. 180–188, 2007.

[3] P. Ogonowska, A. Woźniak, M. K. Pierański, T. Wasylew, P. Kwiek, M. Brasel, M. Grinholc, and J. Nakonieczna, "Application and characterization of light-emitting diodes for photodynamic inactivation of bacteria," *Lighting Research and Technology*, vol. 51, no. 4, pp. 612–624, 2019.

[4] E. Sorbellini, M. Rucco, and F. Rinaldi, "Photodynamic and photobiological effects of light-emitting diode (LED) therapy in dermatological disease: an update," *Lasers in Medical Science*, vol. 33, no. 7, pp. 1431–1439, 2018.

[5] N. N. Houreld, "Shedding light on a new treatment for diabetic wound healing: A review on phototherapy," *The Scientific World Journal*, vol. 2014, 2014.

[6] D. S. Seidman, J. Moise, Z. Ergaz, A. Laor, H. J. Vreman, D. K. Stevenson, and R. Gale, "A prospective randomized controlled study of phototherapy using blue and blue-green light-emitting devices, and conventional halogen-quartz phototherapy," *Journal of Perinatology*, vol. 23, pp. 123–127, 3 2003.

[7] H. J. Vreman, R. J. Wong, and D. K. Stevenson, "Phototherapy: Current Methods and Future Directions," *Seminars*, 2004.

[8] B. C. Wilson and M. S. Patterson, "The physics, biophysics and technology of photodynamic therapy," *Physics in Medicine and Biology*, vol. 53, no. 9, 2008.

[9] R. G. Calderhead, "Review article: The photobiological basics behind light-emitting diode (LED) phototherapy," *Laser Therapy*, vol. 16, no. 2, pp. 97–108, 2007.

[10] T. Dai, A. Gupta, C. K. Murray, M. S. Vrahas, G. P. Tegos, and M. R. Hamblin, "Blue light for infectious diseases: Propionibacterium acnes, Helicobacter pylori, and beyond?," *Drug Resist Updat*, vol. 15, no. 4, pp. 223–236, 2012.

[11] L. Brancaleon and H. Moseley, "Laser and non-laser light sources for photodynamic therapy," *Lasers in Medical Science*, vol. 17, no. 3, pp. 173–186, 2002.

[12] E. M. Kercher, R. T. Lang, B. Q. Spring, E. M. Kercher, K. Zhang, M. Waguespack, R. T. Lang, and A. Olmos, "High-power light-emitting diode array design and assembly for practical photodynamic therapy research," vol. 25, no. May, 2020.

[13] "BiliSoft 2.0 Phototherapy System."

[14] M. S. Nestor, N. Swenson, and A. Macri, "Physical Modalities (Devices) in the Management of Acne," *Dermatologic Clinics*, vol. 34, no. 2, pp. 215–223, 2016.

[15] F. Farrell, E. Xie, B. Guilhabert, A. M. Haughey, P. Connolly, M. D. Dawson, and N. Laurand, "A wearable phototherapy device utilizing micro-LEDs," *Proceedings of the Annual International Conference of the IEEE Engineering in Medicine and Biology Society, EMBS*, no. c, pp. 67–70, 2019.

[16] I. Moreno and R. I. Tzonchev, "Designing light-emitting diode arrays for uniform near-field irradiance," vol. 45, no. 10, pp. 2265–2272, 2006.

[17] Y. Ding, X. Liu, Z.-r. Zheng, P.-f. Gu, P. Zhou, W. Lu, Y. X. Lin, Z. R. Zheng, H. F. Li, and P. F. Gu, "Freeform LED lens for uniform illumination References and links," tech. rep., 2008.

[18] C. Lian, M. Piksa, K. Yoshida, S. Persheyev, K. J. Pawlik, K. Matczyszyn, and I. D. W. Samuel, "Flexible organic light-emitting diodes for antimicrobial photodynamic therapy," *npj Flex Electron*, vol. 3, no. 18, 2019.

[19] C. Ash, M. Dubec, K. Donne, and T. Bashford, "Effect of wavelength and beam width on penetration in light-tissue interaction using computational methods," *Lasers in Medical Science*, vol. 32, pp. 1909–1918, 11 2017.

[20] S. Takezaki, S. Kawana, T. Omi, T. Omi, and S. Sato, "Ultrastructural observations of human skin following irradiation with visible red light-emitting diodes (LEDS): A preliminary in vivo report," *Laser Therapy*, vol. 14, no. 4, pp. 153–159, 2005.

[21] M. A. Trelles, E. Mayayo, L. Miro, J. Rigau, G. Baudin, and R. G. Calderhead, "The action of low reactive level laser therapy (LLLT) on mast cells: a possible pain relief mechanism examined," *LASER THERAPY*, vol. 1, no. 1, pp. 27–30, 1989.

[22] G. Smith, W. G. McGimpsey, M. C. Lynch, I. E. Kochevar, and R. W. Redmond, "An efficient oxygen independent two-photon photosensitization mechanism," *Photochemistry and Photobiology*, vol. 59, pp. 135–139, 2 1994.

[23] T. Karu, "Low-Power Laser Therapy Partial Derepression of Genome of Human Peripheral Lymphocytes: Biological Limitations of Low-Power Laser Effects," in *Biomedical Photonics Handbook*, pp. 1–20, 2003.

[24] R. F. Jackson, G. C. Roche, and S. C. Shanks, "A double-blind, placebo-controlled randomized trial evaluating the ability of low-level laser therapy to improve the appearance of cellulite," *Lasers in Surgery and Medicine*, vol. 45, pp. 141–147, 3 2013.

[25] N. Kuboyama, M. Ohta, Y. Sato, and Y. Abiko, "Anti-inflammatory activities of light emitting diode irradiation on collagen-induced arthritis in mice (a secondary publication)," *Laser Therapy*, vol. 23, no. 3, pp. 191–199, 2014.

[26] M. N. Alba, M. Gerenutti, V. M. H. Yoshida, and D. Grotto, "Clinical comparison of salicylic acid peel and LED-Laser phototherapy for the treatment of Acne vulgaris in teenagers," *Journal of Cosmetic and Laser Therapy*, vol. 19, pp. 49–53, 1 2017.

[27] D. J. Goldberg and B. A. Russell, "Combination blue (415 nm) and red (633 nm) LED phototherapy in the treatment of mild to severe acne vulgaris," *Journal of Cosmetic and Laser Therapy*, vol. 8, pp. 71–75, 1 2006.

[28] H. Serrage, V. Heiskanen, W. M. Palin, P. R. Cooper, M. R. Milward, M. Hadis, and M. R. Hamblin, "Under the spotlight: mechanisms of photobiomodulation concentrating on blue and green light," *Photochemical & Photobiological Sciences*, vol. 18, no. 8, pp. 1877–1909, 2019.

[29] T. Dai, A. Gupta, Y. Y. Huang, R. Yin, C. K. Murray, M. S. Vrahas, M. E. Sherwood, G. P. Tegos, and M. R. Hamblin, "Blue light rescues mice from potentially fatal pseudomonas aeruginosa burn infection: Efficacy, safety, and mechanism of action," *Antimicrobial Agents and Chemotherapy*, vol. 57, no. 3, pp. 1238–1245, 2013.

[30] M. E. Cox, *Handbook of Optics* , vol. 47. McGraw-Hill Education, 3 ed., 1979.

[31] P. A. Jenkins and J. D. Carroll, "How to report low-level laser therapy (LLLT)/photomedicine dose and beam parameters in clinical and laboratory studies," *Photomedicine and Laser Surgery*, vol. 29, no. 12, pp. 785–787, 2011.

[32] R. J. Lanzafame, I. Stadler, A. F. Kurtz, R. Connelly, T. A., P. Brondon, and D. Olson, "Reciprocity of exposure time and irradiance on energy density during photoradiation on wound healing in a murine pressure ulcer model," *Lasers in Surgery and Medicine*, vol. 39, pp. 534–542, 7 2007.

[33] J. Li and G.-Q. Zhang, *Light-Emitting Diodes: Materials, Processes, Devices and Applications*, vol. 4. 2019.

[34] C. M. Bourget, "An Introduction to Light-emitting Diodes," *HortScience*, vol. 43, pp. 1944–1946, 12 2008.

[35] A. V. Arecchi, T. Messadi, and R. J. Koshel, *Field Guide to Illumination*. USA: Society of Photo-Optical Instrumentation Engineers (SPIE), 2007.

[36] *Modeling Sources in LightTools*. Synopsys, 2019.

[37] S. L. Jacques and L. Wang, "Monte Carlo Modeling of Light Transport in Tissues," in *Optical-Thermal Response of Laser-Irradiated Tissue* (A. J. Welch and M. J. C. Van Gemert, eds.), pp. 73–100, Boston, MA: Springer US, 1995.

[38] O. Barajas, A. M. Ballangrud, G. G. Miller, R. B. Moore, and J. Tulip, "Monte Carlo modelling of angular radiance in tissue phantoms and human prostate: PDT light dosimetry," *Physics in Medicine and Biology*, vol. 42, pp. 1675–1687, 9 1997.

[39] L. Wang, S. L. Jacques, and L. Zheng, "MCML-Monte Carlo modeling of light transport in multi-layered tissues," *Computer Methods and Programs in Biomedicine*, 1995.

[40] W. Suthabanditpong, M. Tani, C. Takai, M. Fuji, R. Buntem, and T. Shirai, "Facile fabrication of light diffuser films based on hollow silica nanoparticles as fillers," *Advanced Powder Technology*, vol. 27, no. 2, pp. 454–460, 2016.

[41] H. Kuo, M. Chuang, and C. Lin, "Design correlations for the optical performance of the particle-diffusing bottom diffusers in the LCD backlight unit," *Powder Technology*, vol. 192, pp. 116–121, 5 2009.

[42] Y.-C. Kuo, S.-S. Wang, K.-C. Chang, and H. Chen, "Novel and feasible method for synthesis of monodispersed hollow silicon dioxide submicrospheres," *Journal of Thermoplastic Composite Materials*, vol. 28, no. 8, pp. 1091–1109, 2015.

[43] P. Hu, D. Ai, X. Jiang, and X. Zhang, "Fabrication of hollow silica nanosphere and its application for thermal insulation coating," *Journal of Thermoplastic Composite Materials2*, vol. 33, no. 2, pp. 198–213, 2020.

[44] A. L. Aden and M. Kerker, "Scattering of Electromagnetic Waves from Two Concentric Spheres," *Journal of Applied Physics*, vol. 22, pp. 1242–1246, 10 1951.

[45] M. S. Durkee, G. K. Fletcher, C. Carlson, K. Matheson, S. K. Swift, D. J. Maitland, J. D. Cirillo, and K. C. Maitland, "Light scattering by pulmonary alveoli and airway surface liquid using a concentric sphere model," *Optics Letters*, vol. 43, no. 20, p. 5001, 2018.

[46] C. F. Bohren, "Absorption and scattering of light by small particles," *Absorption and scattering of light by small particles*, 1983.

[47] E. Meng and R. Sheybani, "Insight: Implantable medical devices," *Lab on a Chip*, vol. 14, no. 17, pp. 3233–3240, 2014.